Delayed Frost Growth on Jumping-Drop Superhydrophobic Surfaces

Jonathan B. Boreyko and C. Patrick Collier*

Center for Nanophase Materials Sciences, Oak Ridge National Laboratory, Oak Ridge, Tennessee 37831-6493, United States

ABSTRACT Self-propelled jumping drops are continuously removed from a condensing superhydrophobic surface to enable a micrometric steady-state drop size. Here, we report that subcooled condensate on a chilled superhydrophobic surface are able to repeatedly jump off the surface before heterogeneous ice nucleation occurs. Frost still forms on the superhydrophobic surface due to ice nucleation at neighboring edge defects, which eventually spreads over the entire surface *via* an interdrop frost wave. The growth of this interdrop frost front is shown to be up to 3 times slower on the superhydrophobic surface compared to a control hydrophobic surface, due to the jumping-drop effect dynamically minimizing the average drop size and surface coverage of the condensate. A simple scaling model is developed to relate the success and speed of interdrop ice bridging to the drop size distribution. While other reports of condensation frosting on superhydrophobic surfaces have focused exclusively on liquid–solid ice nucleation for isolated drops, these findings reveal that the growth of frost is an interdrop phenomenon that is strongly coupled to the wettability and drop size distribution of the surface. A jumping-drop superhydrophobic condenser minimized frost formation relative to a conventional dropwise condenser in two respects: preventing heterogeneous ice nucleation by continuously removing subcooled condensate, and delaying frost growth by limiting the success of interdrop ice bridge formation.

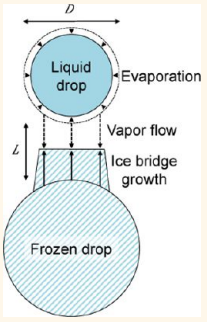

KEYWORDS: superhydrophobic · icephobic · dropwise condensation · jumping drops · frost

The solid contact and heat transfer between water and a supporting substrate are typically minimized when the surface is superhydrophobic, creating the potential for utilizing superhydrophobicity for anti-icing applications.[1] Thus far, most research on icephobicity has focused on deposited drops[2−6] or impacting drops[7−10] on a subzero superhydrophobic surface. When tap water is used, impurities usually trigger ice nucleation as soon as the drop cools to 0 °C.[2] In such cases, a suspended Cassie[11] drop on a superhydrophobic surface exhibits a freezing time up to 3−5 times longer than an equivalent drop on a smooth hydrophobic surface, due to an increased ratio of drop volume to solid−liquid contact area minimizing the heat transfer.[2] When pure water is used, a free energy barrier for heterogeneous ice nucleation enables liquid subcooling, where the probability of freezing at a given temperature increases with the surface wettability and the feature size of the surface roughness.[7,9,10] Subcooled drops typically exhibit delayed freezing on superhydrophobic surfaces compared to hydrophobic or hydrophilic surfaces,[4,7,8,10] although delayed freezing on smooth hydrophilic surfaces such as glass and silicon was also observed when the benefit of reduced surface roughness outweighed the cost of increased wettability.[3,9] In the presence of a chilled air flow, ice nucleation may also occur at the liquid−air interface of a superhydrophobic drop instead of at the substrate.[5]

While the freezing mechanisms of drops placed on smooth and textured surfaces are beginning to be well understood, relatively little is known concerning the freezing of subcooled condensate into frost. Below the triple point, water vapor in the air tends to condense directly into frost, known as deposition. Above the triple point, vapor condenses into liquid, which in the case of a subzero surface will eventually freeze and form a frost layer.[12−14] The freezing of subcooled liquid condensate is known as condensation frosting and is more common than deposition in many practical settings.[14,15] Condensation frosting is especially prevalent for hydrophobic surfaces, as the degree of supersaturation required for direct ice deposition is an order of magnitude larger compared to hydrophilic surfaces.[16] It is therefore of interest to better understand the incipient mechanisms and dynamics of condensation frosting and whether superhydrophobic surfaces could minimize the onset and growth of frost formation.

* Address correspondence to colliercp@ornl.gov.

Received for review November 27, 2012 and accepted January 3, 2013.

Published online January 03, 2013
10.1021/nn3055048

Water vapor condensing onto a superhydrophobic surface with only microscale roughness tends to nucleate within the surface roughness in an impaled Wenzel[17] state, degrading the system's superhydrophobicity.[18−21] In contrast to deposited drops in a suspended Cassie state, condensate drops in an impaled Wenzel state actually exhibit greater liquid−solid contact and heat transfer compared to drops on smooth surfaces. As long as condensate forms in the Wenzel state, superhydrophobic surfaces do not seem effective at minimizing frost formation and adhesion,[22−25] and this frost can even diminish the icephobicity of the surfaces for deposited drops, as well.[2,26,27] More promising are superhydrophobic surfaces with robust nanoscale[28−32] or hierarchical[33−37] roughness, which are capable of forming condensate in a suspended (or partially suspended) Cassie state. These spherical condensate drops exhibit minimal solid contact with the superhydrophobic surface and are even capable of spontaneously jumping off the surface *via* the surface energy harvested from naturally occurring coalescence.[34,38]

Recently, it was observed that cooling robust superhydrophobic surfaces below zero enables the formation of subcooled spherical condensate that exhibits delayed condensation frosting compared to traditional filmwise and dropwise condensers.[13,39−42] It was reported that the increased hydrophobicity and decreased solid−liquid contact area of the spherical condensate was responsible for the delay in the onset of freezing,[13,40,41] analogous to the argument made for deposited drops.[7,9,10] No mention has been made, however, of the *interdrop* freezing dynamics, in which a frozen condensate drop contacts neighboring liquid drops to freeze them, as well, setting off a chain reaction that results in a propagating frost front.[12,14] This interdrop frost front is fundamentally different from the freezing of an isolated drop and is arguably even more important since a single frozen drop can proceed to frost the entire surface *via* interdrop ice propagation. Furthermore, no connection has been made between the jumping-drop dynamics of a superhydrophobic condenser and the delay in condensation frosting.

Here, we report that subcooled jumping-drop condensate on a hierarchical superhydrophobic surface are able to jump off the surface before heterogeneous ice nucleation can occur. Therefore, frost formation does not begin on the superhydrophobic surface at all, but rather at nearby edge defects which proceed to frost the entire surface *via* an interdrop frost wave. The propagation velocity of the interdrop frost growth is found to be up to 3 times slower on the two-tier superhydrophobic surface compared to a smooth hydrophobic surface, by virtue of the jumping-drop effect dynamically minimizing the surface coverage of the subcooled condensate. These findings refine the understanding of frost formation on dropwise condensers: rather than each condensate drop freezing independently due to ice nucleation at the surface, it is instead geometrically coupled to a drop's proximity to surface defects and to the velocity of interdrop frost waves spreading from those defects. Jumping-drop superhydrophobic condensers are useful not only for dynamically removing subcooled condensate before they can freeze but also for minimizing the velocity of the interdrop frost growth that invades the surface from nearby defects.

RESULTS AND DISCUSSION

Condensation frosting was studied by cooling horizontally oriented copper samples (19 × 19 × 0.81 mm) down to −10 or −20 °C on a Peltier stage and observing the formation of condensate and frost with a top-down microscope and digital camera. To compare the frosting performance of traditional dropwise condensation[43] to jumping-drop condensation,[34] smooth and two-tier surfaces were coated with an identical monolayer of 1-hexadecanethiol to create hydrophobic and superhydrophobic surfaces, respectively. The two-tier roughness imparted onto the superhydrophobic surface was composed of galvanically deposited silver particles using a simple dip-coat recipe,[44] the same recipe used in a previous report to characterize the icephobicity of deposited drops[2] and known to produce robust jumping-drop behavior during condensation.[45] The sudden freezing of a subcooled condensate drop was readily identified by a reduction in brightness in the center of the drop and also by the initiation of physical contact with a neighboring drop which was already frozen and responsible for propagating the frost. (See Methods section for more experimental details.)

Dynamic Removal of Subcooled Jumping-Drop Condensate. On the cooled hydrophobic surface, hemispherical ($\theta \approx 100°$) condensate formed and continued to grow to increasingly larger sizes (Figure 1A). On the cooled superhydrophobic surface, spherical ($\theta \approx 160°$) condensate formed and after about 100 s of growth began to rapidly jump out-of-plane from the surface upon coalescence (Figure 1B). Before drops could jump upon coalescence, they typically required growth to a diameter of ∼10 μm. This is consistent with the initial report on jumping drops[34] and is most likely related to the critical growth size required to attain the spherical shape[29] needed for jumping.[38] Once jumping occurred, ∼10 μm condensate were continuously shed from the surface, allowing for the fresh nucleation of smaller condensate. After 5 min of growth, over 85% of drops visible on the superhydrophobic surface were smaller than 20 μm due to jumping-drop removal, in contrast to the hydrophobic surface where every drop was larger than 20 μm (Figure 1C).

For both the −10 and −20 °C cooling temperatures, it was observed that the subcooled condensate on the

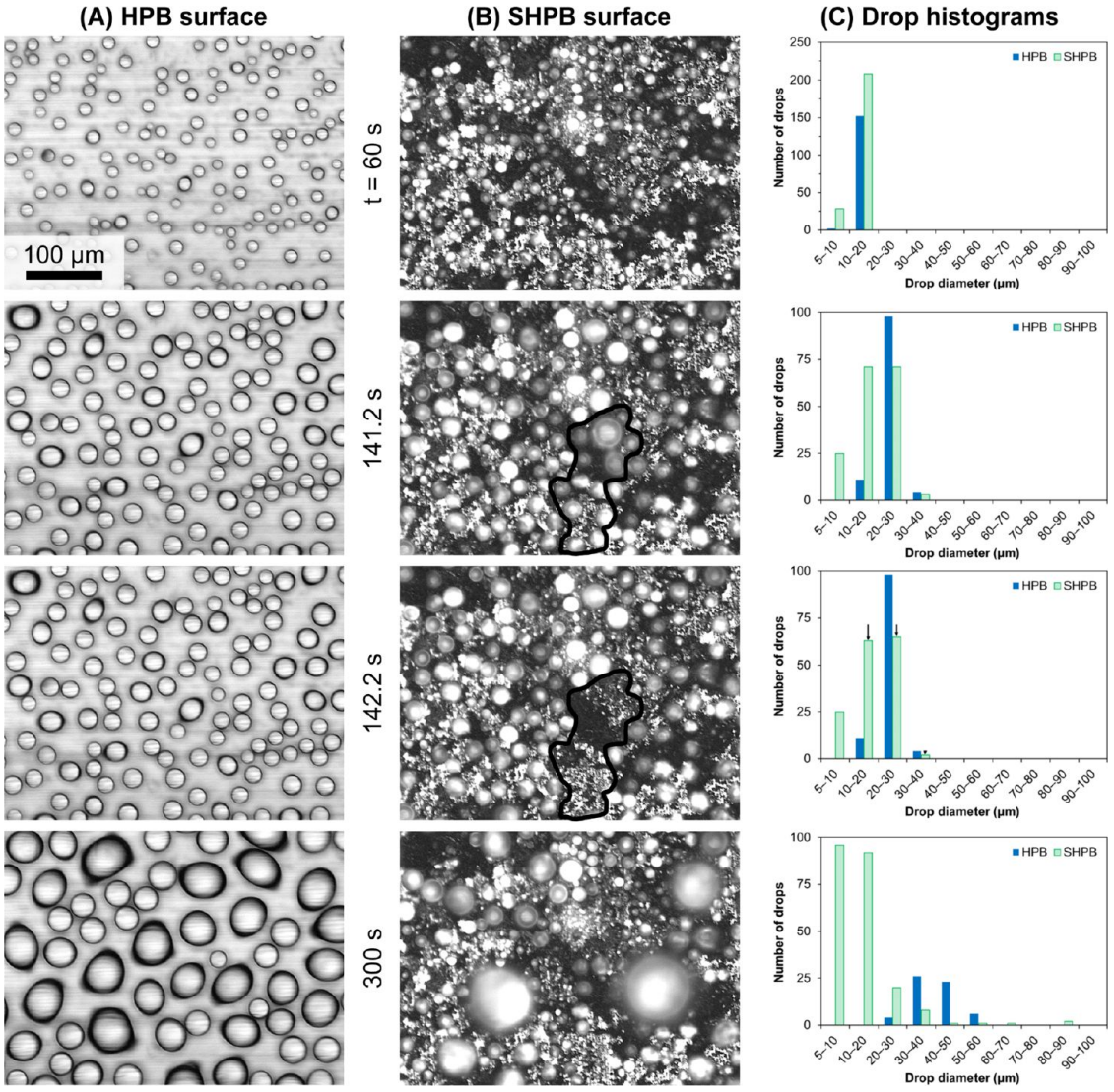

Figure 1. Growth of subcooled condensate on horizontally oriented (A) hydrophobic and (B) superhydrophobic surfaces chilled to −10 °C. While condensate drops were fixed to the hydrophobic surface, drops on the superhydrophobic surface were able to continuously jump off the surface before freezing could occur. This is illustrated by the outlined cluster of drops that jumped between 141.2 and 142.2 s due to several coalescence events. (C) Histograms reveal that the jumping-drop effect minimizes the drop size distribution of the superhydrophobic surface by continuously removing larger condensate. Time zero corresponds to the start of cooling the sample from 12 to −10 °C, which took approximately 45 s. The clusters of small white particles visible in (B) are surface roughness features and should not be mistaken for condensate. Videos of condensate growth at −10 and −20 °C are available in the Supporting Information, videos S1−S4.

superhydrophobic surface were consistently able to jump off the surface before any heterogeneous ice nucleation could occur (Figure 1B). This observation has important implications for long-term frost prevention: freezing is delayed but still inevitable for condensate on superhydrophobic surfaces,[41] but a jumping-drop condenser allows dew drops to dynamically depart the surface before freezing can occur. Dynamically removing subcooled drops by gravity[2,42,46] or bouncing[8] have previously been reported. Distinct advantages of jumping-drop removal include its gravitational independence, early drop removal at micrometric length scales, and its inherent applicability to condensation for frost prevention. The long-term prevention of heterogeneous ice nucleation on the jumping-drop surface could not be confirmed, as the surface was eventually invaded by an interdrop frost front that swept in from defects at the edge of the superhydrophobic copper plate.

Frost Growth. For both the hydrophobic and superhydrophobic condensers used here, the onset of frost always began at condensate located along the edges of the copper sample. Macroscopically, this was evident to the eye by seeing that the white frost layer first appeared along the outer edges of the copper and proceeded to grow inward, such that the center of the sample was always last to frost over. By focusing the microscope on drops at the center of the copper surface, it was observed that ice nucleation never initiated inside the field-of-view, but rather the

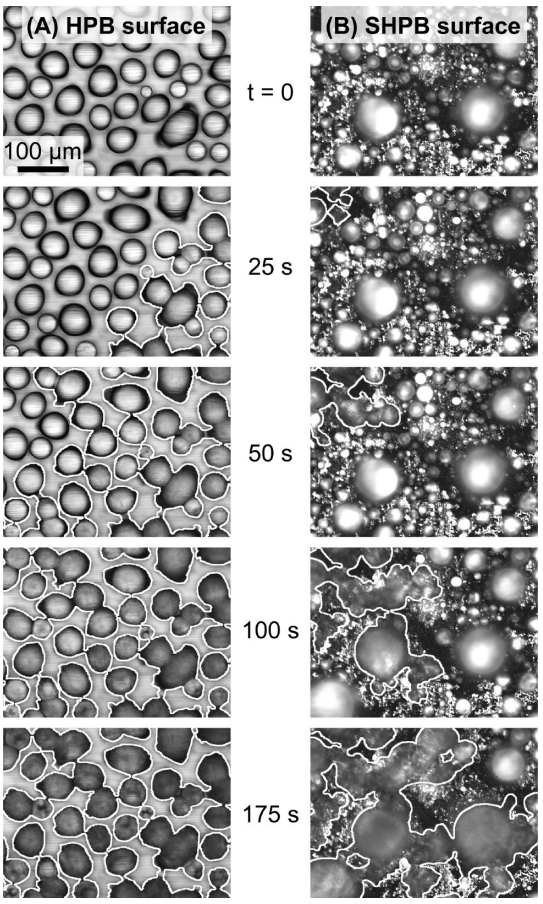

Figure 2. Growth of an invading interdrop frost front on (A) hydrophobic and (B) superhydrophobic surfaces cooled to −10 °C. The interdrop frost front spread over the entire field-of-view of the hydrophobic surface within 55 s, while the jumping-drop superhydrophobic surface delayed the frosting time to 211 s. Time zero corresponds to the onset of interdrop frost growth within the field-of-view of the microscope, and a white outline is provided to help visualize the frozen drops. The gradual darkening of the frozen drops over time is due to the transition from stage-one rapid freezing to stage-two slow freezing.[41] See Supporting Information, videos S5−S8, for movies of interdrop frost growth at −10 and −20 °C.

subcooled drops froze due to an interdrop frost front that swept in from outside the field-of-view (Figure 2). The preferential onset of frost along the rim of the copper samples was due to the abundance of physical and/or chemical defects inherently present along such edges, which provide effective nucleation sites for heterogeneous ice formation. This was confirmed by intentionally damaging a portion of a superhydrophobic surface, in which case frost was also able to initiate at the introduced defects in addition to the edges. While interdrop frost fronts have not been mentioned in previous reports of condensation frosting on superhydrophobic condensers,[40−42] we believe they are the underlying cause for the interconnected wave of frozen drops visibly sweeping through the field-of-view over time.

A consequence of the observed interdrop frosting dynamics is that the delayed icing performance of a dropwise or jumping-drop condenser cannot prevent eventual freezing when neighboring surface defects spread frost across the entire surface. For a given subcooled condensate drop on a surface, its freezing time depends on its distance from the initial ice nucleation site, the time required for ice to nucleate at that site, and on the velocity of the interdrop frost wave that travels from the site to the drop of interest. For example, when the microscope was focused at the center of a copper sample, the field-of-view typically frosted over after 5−7 min of cooling at −10 °C, compared to only 2−3 min when focusing on a portion of the sample only a couple of millimeters away from the edge. Therefore, freezing times are only a useful benchmark when describing ice nucleation at an isolated drop due to its contact with the surface or the air, while the propagation velocity of the interdrop frost front is a more useful metric for characterizing the subsequent frosting of a surface. Previous studies were able to isolate the initial onset of freezing by mechanically sealing a uniformly hydrophobic[41,47] or superhydrophobic[41] condenser from any nearby edges or defects, while this study focuses on interdrop frosting after ice nucleation has already occurred.

The superhydrophobic condenser exhibited significantly slower interdrop frost growth compared to the hydrophobic condenser (Figure 2). While the microscopic growth of the interdrop frost front involves a complex network of drop connections, the growth rate may be generalized as the time required to spread over the entire field-of-view. At −10 °C, the hydrophobic and superhydrophobic surfaces required average times of 58 ± 9 and 170 ± 80 s, respectively, to propagate frost over the field-of-view. This corresponds to frost wave velocities of 7.8 ± 1.1 and 2.8 ± 1.2 μm/s. Therefore, the jumping-drop superhydrophobic surface delays the growth of frost by about a factor of 3 compared to a hydrophobic condenser. Interestingly, when the same procedure was repeated at −20 °C, the difference in frosting velocities was reduced to a factor of 2: 12.4 ± 1.5 μm/s on the hydrophobic surface *versus* 6.2 ± 0.9 μm/s on the superhydrophobic one. To understand this temperature-dependent frosting performance, the underlying mechanism of the interdrop frost growth must first be examined.

Scaling Model for Interdrop Bridging. It was observed using microscopy that when a subcooled condensate drop first became frozen on the hydrophobic or superhydrophobic surface, neighboring drops still in the liquid phase immediately began to evaporate. This sudden evaporation of liquid drops next to frozen drops may seem surprising, given that the water vapor surrounding the chilled surface was supersaturated and otherwise promoted the steady growth of the condensate. It has been previously reported that this phenomenon is caused by the difference in saturation

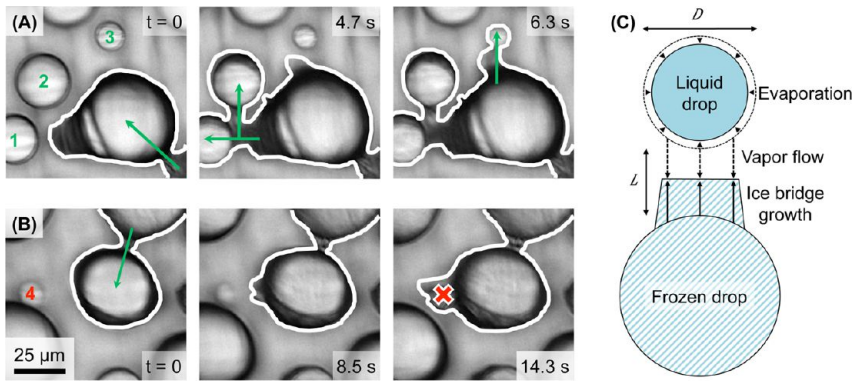

Figure 3. Ice bridge growth from a frozen drop to neighboring liquid drops on a hydrophobic surface chilled to −20 °C. (A) When liquid drops were close enough to a frozen drop, the ice bridge connected to the liquid drops and immediately froze them (drops 1−3). (B) For liquid drops that were small and/or far away from a frozen drop, the liquid drop completely evaporated before a bridge could connect, stopping the local progression of the frost front (drop 4). (C) Schematic of the growth of an ice bridge between a frozen drop and a subcooled liquid drop. The speed and success of bridge formation depend on the interplay between the evaporation rate ($\propto D^2$) and the required mass for bridge completion ($\propto DL$). See Supporting Information, videos S9 and S10.

pressure for water vapor above water *versus* ice, which can induce a vapor pressure gradient with localized subsaturation around water drops located near frozen drops.[12,14] It is possible that the latent heat released by freezing drops could also play a role by locally heating the substrate.

The evaporative water vapor deposited onto the neighboring frozen drop in the form of an ice bridge, which grew along the substrate toward the evaporating liquid drop (Figure 3). When the evaporating liquid drop was sufficiently close to the frozen drop, the ice bridge was able to grow all the way to the liquid drop, freezing it upon contact (Figure 3A). Once frozen, the process began afresh with this new drop's liquid neighbors, continuing the chain reaction until the entire surface was frozen. However, it was also observed that if a liquid drop was sufficiently small or far away from the nearest frozen drop, then it would completely evaporate and disappear before the ice bridge could reach it (Figure 3B). Therefore, the success of interdrop frost growth would appear to be dependent on the diameter of the liquid drop and its separation from the frozen drop (Figure 3C).

The dynamics of a growing ice bridge are complex. Typically, drops have multiple neighbors, promoting the interconnected liquid evaporation and ice growth of several drops at once. Even under the simplified case of a single frozen drop next to a liquid drop, the bridge growth still depends on multiple three-dimensional and time-dependent parameters such as the vapor pressure distribution, evaporation rate, ice growth rate, and the geometry of an ice bridge growing along the surface. The thermal conductivity of the substrate is also likely to be important, as the initial freezing of a drop generates latent heat that must be removed into the substrate or by evaporation.[6] To simplify this problem, a combination of two-dimensional scaling analysis and statistical analysis will be employed here to make some generalized correlations between the frost growth rate and the drop size distribution.

For a liquid drop of initial diameter D neighboring a frozen drop, its evaporation rate J_e (kg/s) will be proportional to its overall surface area:

$$J_e \propto D^2 \quad (1)$$

While the supersaturated water vapor in the ambient did promote the overall growth of the frost layer, the initial interdrop frosting process was deduced to be primarily fed by the evaporating water drops for three reasons. First, the ice bridges always grew directly toward the evaporating liquid drops and could not grow elsewhere. Second, the growth rate of an ice bridge was observed to be approximately equal to the evaporation rate of its neighboring liquid drop (Figure 3). Finally, as soon as the evaporating liquid drops had also frozen over (or disappeared), the subsequent growth of the frost sheet was reoriented out-of-plane toward the ambient, as opposed to the wholly lateral growth of the initial interdrop frosting. Under this assumption that the water vapor from the evaporating drops efficiently deposits on the frozen drops, eq 1 may also be used to estimate the growth rate of an ice bridge:

$$J_i \sim J_e \quad (2)$$

Equations 1 and 2 suggest that the area of the liquid drop, rather than the area of the frozen drop, primarily determines the growth rate of the ice bridge. This was evidenced by experimental observations where a frozen drop, equidistant to several neighboring liquid drops of varying size, was able to bridge to larger liquid drops faster.

The area and mass of a completed ice bridge are difficult to characterize, but in two dimensions, both are roughly proportional to the interdrop separation (L) and to the diameter of the evaporating liquid

drop (see Figure 3):

$$A_{bridge} \propto m_{bridge} \propto DL \quad (3)$$

The time required for successful bridge formation scales as

$$t_{bridge} \sim \frac{m_{bridge}}{J_i} \quad (4)$$

which from eqs 1−3 is proportional to a dimensionless coefficient:

$$S^* \sim \frac{L}{D} \quad (5)$$

This dimensionless coefficient, S^*, will be referred to as the bridging parameter. For values of $S^* < 1$, an ice bridge is expected to successfully connect a frozen drop to its neighboring liquid drop (as in Figure 3A). When $S^* > 1$, the area required for bridge completion becomes larger than the total surface area of the evaporating liquid drop, causing the drop to disappear entirely before bridging is achieved (as in Figure 3B). This effectively halts the local advancement of the inter-drop frost front, which must now rely on other paths to continue the chain reaction. To test the effectiveness of eq 5, the values of D, S^*, and t_{bridge} were systematically measured for drops on both the hydrophobic and superhydrophobic surfaces.

Effect of Wettability on Drop Size Distribution and Frost Growth Rate. The bridging parameter (S^*) implies that the drop size distribution should govern the velocity of the frost front. The average diameter, $\langle D \rangle$, and projected surface coverage, ε^2, of subcooled condensate were plotted over time for the hydrophobic and superhydrophobic surfaces at −10 °C (Figure 4A) and −20 °C (Figure 4B). Times selected for drop measurement spanned from the end of the cooling transient (45 s for −10 °C and 75 s for −20 °C) to the onset of inter-drop frost growth invading the field-of-view. The two-tier surface roughness of the superhydrophobic condenser made it difficult to focus at magnifications larger than 20×. At this magnification, only drops with diameters of 5 μm or larger were counted to avoid inconsistencies in resolving smaller drops.

Growth of dropwise condensate on hydrophobic and superhydrophobic surfaces under steady-state conditions is known to exhibit power-law growth:

$$\langle D \rangle \sim t^{\alpha} \quad (6)$$

where $\alpha \approx 0.33$ during stage-one growth of isolated condensate[19,48] and $\alpha \approx 0.75-1$ for stage-two growth where frequent coalescence events occur.[19,34,49] Exclusive to a robust superhydrophobic condenser, a third stage exhibiting zero growth, $\alpha \approx 0$, occurs at $\langle D \rangle \approx 10$ μm due to the onset of the jumping-drop effect, which clears drops from the surface to provide continuous dropwise condensation.[34] These trends are observed for the subcooled condensate measured

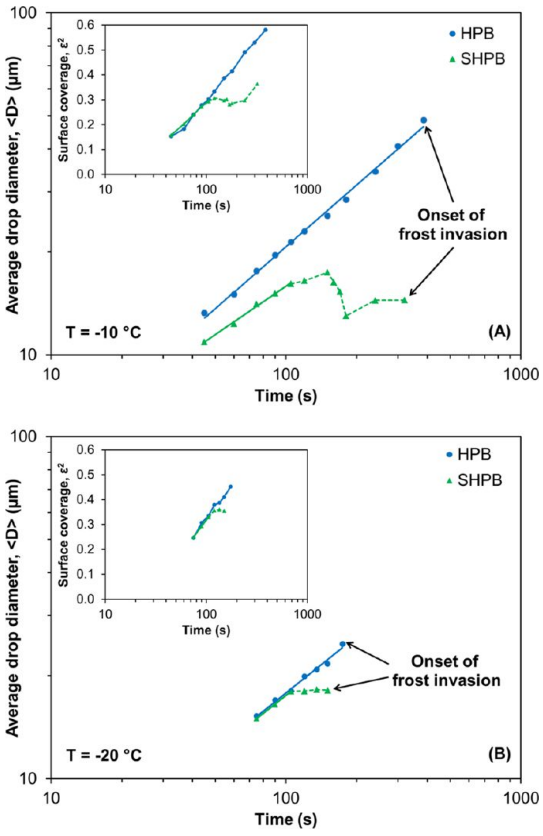

Figure 4. The average drop diameter and surface coverage (inset) of subcooled condensate on chilled hydrophobic and superhydrophobic surfaces diverged over time due to the jumping-drop effect. Solid trendlines represent power-law growth, while dotted lines represent jumping-drop behavior exclusive to the superhydrophobic condenser. The difference in drop size distribution was more pronounced at (A) −10 °C compared to (B) −20 °C, due to the later arrival of frost.

here, where the hydrophobic surface locks into sustained stage-two power-law growth while the superhydrophobic surface levels off to a constant drop diameter after about 100 s of growth (Figure 4). The fitted power-law slopes of the stage-two growth on the hydrophobic and superhydrophobic substrates were between $\alpha \approx 0.5$ and 0.6, slightly lower than expected. This is most likely due to the inability to observe condensate smaller than 5 μm, creating artificially large values of $\langle D \rangle$ at earlier time scales. When only considering times of 3 min and later on the hydrophobic surface at −10 °C, where all drops are large and visible, a more standard growth law of $\alpha \approx 0.71 \pm 0.05$ is recovered, where the uncertainty corresponds to a 95% confidence interval in the power-law fitting.

Once jumping-drop behavior begins, the drop size distribution on the superhydrophobic surface diverges from that of the hydrophobic condenser (Figure 4). For all times proceeding the onset of jumping, this time-dependent divergence scales with

$$\frac{\langle D_{HPB} \rangle}{\langle D_{SHPB} \rangle} \sim \frac{t^{\alpha}}{\langle D_{SHPB} \rangle} \quad (7)$$

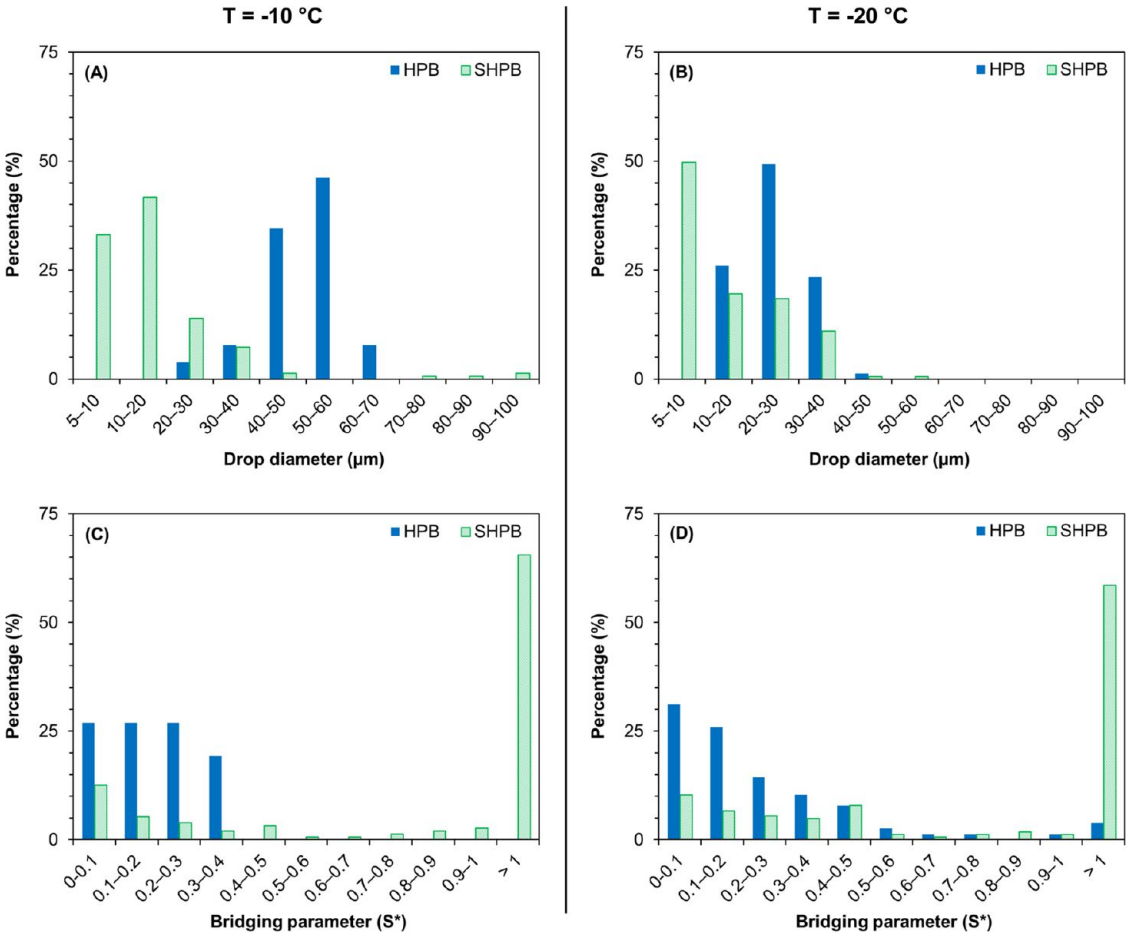

Figure 5. Histograms of the liquid drop diameter (*D*) and the bridging parameter (*S) during ice bridge growth between a frozen drop and a liquid drop on hydrophobic and superhydrophobic condensers. (A) Due to the jumping-drop effect, 75% of superhydrophobic condensate were smaller than 20 μm during interdrop frost growth at −10 °C, while every drop on the hydrophobic condenser was larger than 20 μm. (B) Discrepancy in drop size distribution was less pronounced for the surfaces cooled to −20 °C, due to an earlier arrival of frost. (C,D) On the superhydrophobic surfaces, about 2/3 of drops exhibited *S** > 1 with an incomplete ice bridge, compared to the hydrophobic surfaces where almost every ice bridge between drops was successfully completed.**

where $\alpha \approx 1$ and $\langle D_{SHPB} \rangle \approx 10$ μm.[34] For the case of subcooled condensate, the growth time is bounded by the arrival of frost. This is why the difference in average drop size between the hydrophobic and superhydrophobic surfaces was much greater during interdrop frosting at −10 °C, compared to −20 °C where the frost front arrived much earlier (Figure 4). This greater discrepancy in drop size distribution between the two surfaces at −10 °C was the reason why the difference in frost growth velocity was more pronounced compared to −20 °C.

To relate interdrop frost growth to the drop size distribution of the surfaces, the liquid drop diameter (*D*) and bridging parameter (*S**) were plotted in histograms for each interdrop ice bridge growing within the field-of-view of the microscope (Figure 5). For both the hydrophobic and superhydrophobic surfaces, the liquid drops exhibited an unpinned, receding contact line during evaporation (see videos S5−S10 in the Supporting Information). As a result, the final length (*L*) of a completed ice bridge was typically larger than the initial separation between the frozen drop and liquid drop and was measured accordingly at the time of contact. The later arrival of frost on the samples cooled to −10 °C allowed the jumping-drop surface to exhibit a significant difference in *D* compared to the hydrophobic surface. Measuring *D* as the diameter of a liquid drop immediately before the onset of evaporation triggered by the freezing of a neighboring drop gave $D_{avg} \approx 49$ μm on the hydrophobic surface and $D_{avg} \approx 17$ μm on the superhydrophobic surface. This divergence in *D* greatly affected the effectiveness of ice bridging: the bridging parameter was $S^*_{avg} \approx 0.18$ on the hydrophobic surface and $S^*_{avg} \approx 1.81$ on the superhydrophobic surface, an order of magnitude difference. The earlier arrival of frost on the −20 °C slightly decreased the discrepancy in frost growth, with $D_{avg} \approx 26$ μm and $S^*_{avg} \approx 0.26$ on the hydrophobic surface and $D_{avg} \approx 15$ μm and $S^*_{avg} \approx 1.76$ on the superhydrophobic surface.

The uniquely large values of *S** on the jumping-drop superhydrophobic surface served to decrease

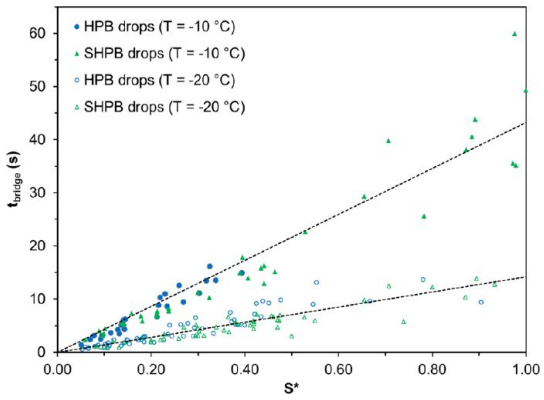

Figure 6. For drops on the hydrophobic and superhydrophobic surfaces where $S^* < 1$, an ice bridge was successfully grown from a frozen drop to a liquid drop over a period of time (t_{bridge}) directly proportional to S^*. Trendlines correspond to slopes of $t_{bridge}/S^* = 43$ s at −10 °C and $t_{bridge}/S^* = 14$ s at −20 °C. Time zero corresponds to the initial freezing of the drop responsible for growing the ice bridge. The spread in data for large values of S^* at −10 °C are likely a result of the long times (>30 s) and lengths required for bridge completion, making their growth especially susceptible to competing effects from additional drops.

the overall frost growth velocity in two different ways. About 2/3 of the superhydrophobic drops exhibited $S^* > 1$ (Figure 5), and in every case, it was observed that these drops evaporated before the ice bridge could connect and continue the chain reaction. As a result, the interdrop frost front could only spread through 1/3 of all drop interactions, significantly reducing the robustness of the propagating network compared to the hydrophobic surface. When $S^* < 1$, the time required for bridge completion was found to be proportional to the value of S^* for both the hydrophobic and superhydrophobic surfaces, verifying eq 5 (Figure 6). At −10 °C, $t_{bridge}/S^* = 43 \pm 14$ s for all drops on both surfaces where $S^* < 1$, with the uncertainty corresponding to a 95% confidence interval. At −20 °C, $t_{bridge}/S^* = 14 \pm 7$ s for drops with $S^* < 1$, revealing that the rate of ice bridge growth is dependent on the degree of subcooling. This similarity in the growth rate of ice bridges between the hydrophobic and superhydrophobic surfaces rules out the possibility of surface features causing the difference in frost growth, verifying that it is instead related to the drop distribution. Even when $S^* < 1$ and ice bridging is successful, the range of values for S^* was larger with the superhydrophobic surface compared to the hydrophobic surface (especially at −10 °C, see Figure 6). This means that the superhydrophobic surface also has an advantage for the cases when interdrop frosting is successful, as it requires a longer time on average to complete an ice bridge, further delaying the growth of frost compared to traditional surfaces.

While the jumping-drop effect is fundamentally independent of gravity,[34] the surface orientation does affect the subsequent drop dynamics and merits a brief discussion. A horizontal orientation was used here to isolate the growth of condensate and frost from gravitational effects; as a result, jumping condensate eventually fell back to the surface. In most cases, the falling drops were able to repeatedly bounce along the substrate, triggering new coalescence events along the way that provided additional kinetic energy, until falling off the edge of the sample.[34] However, on occasion, a drop became immobile upon returning to the surface, which was responsible for two of the four drops larger than $D > 50$ μm in the field-of-view of the superhydrophobic condenser used here (Figure 1B,C). Aside from increasing the drop size distribution, the return of falling condensate is not expected to significantly affect the interdrop frosting dynamics characterized here, as no drops were observed to fall into the field-of-view during frost growth. Since the direction of jumping is always perpendicular to the surface,[38] the problem of returning condensate could be avoided in the future by utilizing a vertical or upside-down orientation, or alternatively by placing a superhydrophilic collector directly opposite of the condensing sample.[45] The other two condensate drops larger than $D > 50$ μm on the superhydrophobic surface (Figure 1B,C) were due to the wide disparity in size between a group of coalescing drops, which can fail to produce enough energy to propel the drops off the surface.[37] Regardless of the occasional large drop on the superhydrophobic surface, the jumping-drop effect minimizes the size of the vast majority of condensate on the surface over time (Figure 1C, 5) even without the assistance of gravitational removal. Aside from using nanoscale roughness,[30,32] it is still an open question how to optimize and characterize the robustness of jumping-drop condensation, which has strong implications for phase-change heat transfer,[31,33−36] planar thermal diodes,[45] and frost prevention (as shown here).

CONCLUSION

Condensation frosting on hydrophobic and superhydrophobic dropwise condensers was found to be primarily caused by interdrop frost waves, which initiated at defects along the edges of the samples and swept across the entire surface in a chain reaction. This finding suggests that using hydrophobic or superhydrophobic surfaces to delay heterogeneous ice nucleation does not prevent the freezing of drops by an interdrop frost front, which only requires a single defect on the condensing surface to nucleate and spread. However, the use of a jumping-drop superhydrophobic condenser was found to minimize the formation of frost in two different ways. First, subcooled condensate was able to continuously jump off the superhydrophobic surface at micrometric drop sizes of 10−100 μm before heterogeneous ice nucleation could occur. Second, while the invasion of interdrop frost from neighboring defects was inevitable, this frost growth was 3 times slower on the superhydrophobic surface compared to the hydrophobic one, by virtue of the jumping-drop

effect maximizing the separation between drops to minimize the success of ice bridging. The small and steady-state drop size distribution of the jumping-drop superhydrophobic surface resulted in consistently slow interdrop frost propagation regardless of how long condensation had been forming before the onset of freezing, in contrast to the hydrophobic surface where the drop size and frost velocity both grew continually with time. The growth of frost on a nonwetting surface is therefore a phenomenon involving multiple length scales, where nanoscale surface roughness defines the drop size distribution of microscopic condensate,[30,32] which in turn governs the interdrop ice bridging responsible for spreading frost over macroscopic areas.

METHODS

Fabrication of Hydrophobic and Superhydrophobic Samples. A 0.81 mm thick sheet of copper alloy 101 was cut into 19 × 19 mm wafers. All wafers were degreased in acetone for 10 min, immersed in ethanol for 10 min, and then rinsed with deionized water. To impart roughness onto the superhydrophobic samples, the copper was immersed in 10 mM $AgNO_3$ for 10 min, which galvanically deposited micro- and nanoparticles onto the copper (see Figure 2 in ref 45). All samples were coated with a hydrophobic monolayer by immersion in 2 mM of 1-hexadecanethiol in ethanol for 15 min.

Experimental Setup. A copper sample was thermally bonded onto a Peltier stage (Deben MK3 Coolstage) using a thermal paste. All experiments were performed in a clean room with an ambient temperature of 22 ± 1 °C and relative humidity of 45 ± 3%. The sample was initially held under a 20× microscope (Olympus BX51) at a temperature of 12 °C, just over the dew point of 10 °C to prevent condensation from forming. The stage was then cooled to −10 or −20 °C, and the resulting condensation frosting was captured with a digital camera (QIClick) at an acquisition rate of 19.1 fps. The surface temperatures of −10 and −20 °C corresponded to supersaturation degrees (SSD) of 3.2 and 8.5, respectively, where SSD = $(P_{v,ambient} - P_{v,sat})/P_{v,sat}$.[16]

The time required for cooling down to steady-state was 45 s for −10 °C and 75 s for −20 °C. For Figures 1 and 4, which depict the growth of subcooled condensate, time zero refers to the onset of cooling and to the initiation of the recorded video. For Figure 2, time zero corresponds to the first moment where the frost wave visibly intrudes into the field-of-view of the microscope. The overall velocity of the frost front was approximated as the time required for frost to completely spread over the field-of-view divided by the width of the field-of-view (449 μm). Three fresh hydrophobic and superhydrophobic samples were used at each temperature to obtain uncertainties within a 95% confidence limit for the overall frost velocities.

Characterization of Condensation Frosting. The diameters (D) and interdrop separations (L) of all drops visible in the field-of-view were manually measured using ImageJ. The surface coverage was calculated by fitting circles around the projected area of every drop and dividing the resulting total by the projected area of the field-of-view. For large drops on the hydrophobic surface with non-uniform perimeters, D was measured as the smallest possible drop diameter. For the superhydrophobic surface, the measured diameter and surface area of each drop corresponded to its maximum projected size, as opposed to its contact line with the surface. When $S^* < 1$, L was measured as the final length of the ice bridge connecting a frozen drop to its neighboring liquid drop, taking into account the partial evaporation of the liquid drop before contact was made. When $S^* > 1$, the ice bridge could not be completed, and L was measured as the total separation between the edge of the frozen drop and the center of the evaporated liquid drop, regardless of the final length of the failed ice bridge. To ensure accuracy, only drops with diameters of $D > 5$ μm were measured. To distinguish blurry drops from surface features, each time stamp was compared to previous time stamps when necessary. Measured values of S^* used in Figure 6 did not include drops where $L < 2$ μm, as the values of L and t_{bridge} were too small to accurately plot.

Conflict of Interest: The authors declare no competing financial interest.

Acknowledgment. The authors acknowledge S. Retterer and J. Salazar for helpful discussions. This research was conducted at the Center for Nanophase Materials Sciences, which is sponsored at Oak Ridge National Laboratory by the Scientific User Facilities Division, Office of Basic Energy Sciences, U.S. Department of Energy.

Supporting Information Available: Ten videos showing subcooled condensation and frost growth on hydrophobic and superhydrophobic surfaces. This material is available free of charge *via* the Internet at http://pubs.acs.org.

REFERENCES AND NOTES

1. Meuler, A. J.; McKinley, G. H.; Cohen, R. E. Exploiting Topographical Texture To Impart Icephobicity. *ACS Nano* **2010**, *4*, 7048–7052.
2. Tourkine, P.; Merrer, M. L.; Quere, D. Delayed Freezing on Water Repellent Materials. *Langmuir* **2009**, *25*, 7214–7216.
3. Yin, L.; Xia, Q.; Xue, J.; Yang, S.; Wang, Q.; Chen, Q. *In Situ* Investigation of Ice Formation on Surfaces with Representative Wettability. *Appl. Surf. Sci.* **2010**, *256*, 6764–6769.
4. Guo, P.; Zheng, Y.; Wen, M.; Song, C.; Lin, Y.; Jiang, L. Icephobic/Anti-icing Properties of Micro/Nanostructured Surfaces. *Adv. Mater.* **2012**, *24*, 2642–2648.
5. Jung, S.; Tiwari, M. K.; Doan, N. V.; Poulikakos, D. Mechanism of Supercooled Droplet Freezing on Surfaces. *Nat. Commun.* **2012**, *3*, 615.
6. Jung, S.; Tiwari, M. K.; Poulikakos, D. Frost Halos from Supercooled Water Droplets. *Proc. Natl. Acad. Sci. U.S.A.* **2012**, *109*, 16073–16078.
7. Cao, L.; Jones, A. K.; Sikka, V. K.; Wu, J.; Gao, D. Anti-icing Superhydrophobic Coatings. *Langmuir* **2009**, *25*, 12444–12448.
8. Mishchenko, L.; Hatton, B.; Bahadur, V.; Taylor, J. A.; Krupenkin, T.; Aizenberg, J. Design of Ice-Free Nanostructured Surfaces Based on Repulsion of Impacting Water Droplets. *ACS Nano* **2010**, *4*, 7699–7707.
9. Jung, S.; Dorrestijn, M.; Raps, D.; Das, A.; Megaridis, C. M.; Poulikakos, D. Are Superhydrophobic Surfaces Best for Icephobicity? *Langmuir* **2011**, *27*, 3059–3066.
10. Alizadeh, A.; Yamada, M.; Li, R.; Shang, W.; Otta, S.; Zhong, S.; Ge, L.; Dhinojwala, A.; Conway, K. R.; Bahadur, V.; *et al.* Dynamics of Ice Nucleation on Water Repellent Surfaces. *Langmuir* **2012**, *28*, 3180–3186.
11. Cassie, A. B. D.; Baxter, S. Wettability of Porous Surfaces. *Trans. Faraday Soc.* **1944**, *40*, 546–550.
12. Hoke, J. L.; Georgiadis, J. G.; Jacobi, A. M. Effect of Substrate Wettability on Frost Properties. *J. Thermophys. Heat Transfer* **2004**, *18*, 228–235.
13. Wang, H.; Tang, L.; Wu, X.; Dai, W.; Qiu, Y. Fabrication and Anti-frosting Performance of Super Hydrophobic Coating Based on Modified Nano-Sized Calcium Carbonate and Ordinary Polyacrylate. *Appl. Surf. Sci.* **2007**, *253*, 8818–8824.
14. Dooley, J. B. Determination and Characterization of Ice Propagation Mechanisms on Surfaces Undergoing Dropwise Condensation. Ph.D. Thesis, Texas A&M, 2010.
15. Hobbs, P. V. *Ice Physics*; Clarendon Press: Oxford, England, 1974.
16. Na, B.; Webb, R. L. A Fundamental Understanding of Factors Affecting Frost Nucleation. *Int. J. Heat Mass Transfer* **2003**, *46*, 3797–3808.

17. Wenzel, R. N. Resistance of Solid Surfaces to Wetting by Water. *Ind. Eng. Chem.* **1936**, *28*, 988–994.
18. Lafuma, A.; Quere, D. Superhydrophobic States. *Nat. Mater.* **2003**, *2*, 457–460.
19. Narhe, R. D.; Beysens, D. A. Nucleation and Growth on a Superhydrohobic Grooved Surface. *Phys. Rev. Lett.* **2004**, *93*, 076103.
20. Cheng, Y. T.; Rodak, D. E. Is the Lotus Leaf Superhydrophobic? *Appl. Phys. Lett.* **2005**, *86*, 144101.
21. Wier, K. A.; McCarthy, T. J. Condensation on Ultrahydrophobic Surfaces and Its Effect on Droplet Mobility: Ultrahydrophobic Surfaces Are Not Always Water Repellant. *Langmuir* **2006**, *22*, 2433–2436.
22. Varanasi, K. K.; Deng, T.; Smith, J. D.; Hsu, M.; Bhate, N. Frost Formation and Ice Adhesion on Superhydrophobic Surfaces. *Appl. Phys. Lett.* **2010**, *97*, 234102.
23. Kulinich, S. A.; Farhadi, S.; Nose, K.; Du, X. W. Superhydrophobic Surfaces: Are They Really Ice-Repellent? *Langmuir* **2011**, *27*, 25–29.
24. Farhadi, S.; Farzaneh, M.; Kulinich, S. A. Anti-icing Performance of Superhydrophobic Surfaces. *Appl. Surf. Sci.* **2011**, *257*, 6424–6429.
25. Stone, H. A. Ice-Phobic Surfaces That Are Wet. *ACS Nano* **2012**, *6*, 6536–6540.
26. Karmouch, R.; Ross, G. G. Experimental Study on the Evolution of Contact Angles with Temperature near the Freezing Point. *J. Phys. Chem. C* **2010**, *114*, 4063–4066.
27. He, M.; Li, H.; Wang, J.; Song, Y. Superhydrophobic Surface at Low Surface Temperature. *Appl. Phys. Lett.* **2011**, *98*, 093118.
28. Lau, K. K. S.; Bico, J.; Teo, K. B. K.; Chhowalla, M.; Amaratunga, G. A. J.; Milne, W. I.; McKinley, G. H.; Gleason, K. K. Superhydrophobic Carbon Nanotube Forests. *Nano Lett.* **2003**, *3*, 1701–1705.
29. Rykaczewski, K. Microdroplet Growth Mechanism during Water Condensation on Superhydrophobic Surfaces. *Langmuir* **2012**, *28*, 7720–7729.
30. Rykaczewski, K. How Nanorough Is Rough Enough To Make a Surface Superhydrophobic during Water Condensation? *Soft Matter* **2012**, *8*, 8786–8794.
31. Miljkovic, N.; Enright, R.; Wang, E. N. Effect of Droplet Morphology on Growth Dynamics and Heat Transfer during Condensation on Superhydrophobic Nanostructured Surfaces. *ACS Nano* **2012**, *6*, 1776–1785.
32. Enright, R.; Miljkovic, N.; Al-Obeidi, A.; Thompson, C. V.; Wang, E. N. Condensation on Superhydrophobic Surfaces: The Role of Local Energy Barriers and Structure Length Scale. *Langmuir* **2012**, *28*, 14424–14432.
33. Chen, C. H.; Cai, Q.; Tsai, C.; Chen, C. L.; Xiong, G.; Yu, Y.; Ren, Z. Dropwise Condensation on Superhydrophobic Surfaces with Two-Tier Roughness. *Appl. Phys. Lett.* **2007**, *90*, 173108.
34. Boreyko, J. B.; Chen, C. H. Self-Propelled Dropwise Condensate on Superhydrophobic Surfaces. *Phys. Rev. Lett.* **2009**, *103*, 184501.
35. Chen, X.; Wu, J.; Ma, R.; Hua, M.; Koratkar, N.; Yao, S.; Wang, Z. Nanograssed Micropyramidal Architectures for Continuous Dropwise Condensation. *Adv. Funct. Mater.* **2011**, 4617–4623.
36. Cheng, J.; Vandadi, A.; Chen, C. L. Condensation Heat Transfer on Two-Tier Superhydrophobic Surfaces. *Appl. Phys. Lett.* **2012**, *101*, 131909.
37. He, M.; Zhou, X.; Zeng, X.; Cui, D.; Zhang, Q.; Chen, J.; Li, H.; Wang, J.; Cao, Z.; Song, Y.; *et al.* Hierarchically Structured Porous Aluminum Surfaces for High-Efficient Removal of Condensed Water. *Soft Matter* **2012**, *8*, 2680–2683.
38. Boreyko, J. B.; Chen, C. H. Self-Propelled Jumping Drops on Superhydrophobic Surfaces. *Phys. Fluids* **2010**, *22*, 091110.
39. He, M.; Wang, J.; Li, H.; Jin, X.; Wang, J.; Liu, B.; Song, Y. Super-Hydrophobic Film Retards Frost Formation. *Soft Matter* **2010**, *6*, 2396–2399.
40. He, M.; Wang, J.; Li, H.; Song, Y. Super-Hydrophobic Surfaces to Condensed Micro-Droplets at Temperatures below the Freezing Point Retard Ice/Frost Formation. *Soft Matter* **2011**, *7*, 3993–4000.
41. Zhang, Q.; He, M.; Zeng, X.; Li, K.; Cui, D.; Chen, J.; Wang, J.; Song, Y.; Jiang, L. Condensation Mode Determines the Freezing of Condensed Water on Solid Surfaces. *Soft Matter* **2012**, *8*, 8285–8288.
42. Zhang, Y.; Yu, X.; Wu, H.; Wu, J. Facile Fabrication of Superhydrophobic Nanostructures on Aluminum Foils with Controlled-Condensation and Delayed-Icing Effects. *Appl. Surf. Sci.* **2012**, *258*, 8253–8257.
43. Rose, J. W. Dropwise Condensation Theory and Experiment: A Review. *Proc. Inst. Mech. Eng., Part A* **2002**, *216*, 115–128.
44. Larmour, I. A.; Bell, S. E. J.; Saunders, G. C. Remarkably Simple Fabrication of Superhydrophobic Surfaces Using Electroless Galvanic Deposition. *Angew. Chem., Int. Ed.* **2007**, *46*, 1710–1712.
45. Boreyko, J. B.; Zhao, Y.; Chen, C. H. Planar Jumping-Drop Thermal Diodes. *Appl. Phys. Lett.* **2011**, *99*, 234105.
46. Kim, P.; Wong, T. S.; Alvarenga, J.; Kreder, M. J.; Adorno-Martinez, W. E.; Aizenberg, J. Liquid-Infused Nanostructured Surfaces with Extreme Anti-ice and Anti-frost Performance. *ACS Nano* **2012**, *6*, 6569–6577.
47. Li, K.; Xu, S.; Shi, W.; He, M.; Li, H.; Li, S.; Zhou, X.; Wang, J.; Song, Y. Investigating the Effects of Solid Surfaces on Ice Nucleation. *Langmuir* **2012**, *28*, 10749–10754.
48. Viovy, J. L.; Beysens, D.; Knobler, C. M. Scaling Description for the Growth of Condensation Patterns on Surfaces. *Phys. Rev. A* **1988**, *37*, 4965–4970.
49. Beysens, D.; Knobler, C. M. Growth of Breath Figures. *Phys. Rev. Lett.* **1986**, *57*, 1433–1436.